Can We Observe Nonperturbative Vacuum Shifts in Cavity QED?

Rocío Sáez-Blázquez,[1] Daniele de Bernardis,[2] Johannes Feist,[3] and Peter Rabl[1,4,5,6]

[1]*Vienna Center for Quantum Science and Technology, Atominstitut, TU Wien, 1020 Vienna, Austria*
[2]*INO-CNR BEC Center and Dipartimento di Fisica, Università di Trento, I-38123 Povo, Italy*
[3]*Departamento de Física Teórica de la Materia Condensada and Condensed Matter Physics Center (IFIMAC), Universidad Autónoma de Madrid, E-28049 Madrid, Spain*
[4]*Technical University of Munich, TUM School of Natural Sciences, Physics Department, 85748 Garching, Germany*
[5]*Walther-Meißner-Institut, Bayerische Akademie der Wissenschaften, 85748 Garching, Germany*
[6]*Munich Center for Quantum Science and Technology (MCQST), 80799 Munich, Germany*

(Received 23 December 2022; accepted 2 June 2023; published 7 July 2023)

We address the fundamental question of whether or not it is possible to achieve conditions under which the coupling of a single dipole to a strongly confined electromagnetic vacuum can result in nonperturbative corrections to the dipole's ground state. To do so we consider two simplified, but otherwise rather generic cavity QED setups, which allow us to derive analytic expressions for the total ground-state energy and to distinguish explicitly between purely electrostatic and genuine vacuum-induced contributions. Importantly, this derivation takes the full electromagnetic spectrum into account while avoiding any ambiguities arising from an *ad hoc* mode truncation. Our findings show that while the effect of confinement *per se* is not enough to result in substantial vacuum-induced corrections, the presence of high-impedance modes, such as plasmons or engineered LC resonances, can drastically increase these effects. Therefore, we conclude that with appropriately designed experiments it is at least in principle possible to access a regime where light-matter interactions become nonperturbative.

DOI: 10.1103/PhysRevLett.131.013602

The first theoretical prediction of the Lamb shift by Bethe in 1947 [1] was an important milestone of modern physics. Not only did he show that the quantized electromagnetic vacuum leads to an observable energy shift in the hydrogen spectrum, but also how a finite value for this shift can be obtained from a divergent perturbation theory through renormalization. In recent years, vacuum-induced modifications of molecular properties have regained considerable attention in the context of cavity QED [2–7], where the coupling of matter to individual electromagnetic modes is strongly enhanced by a tight confinement of the field. It has been speculated that under such *ultrastrong* coupling conditions [3,4], the electromagnetic vacuum could change the rate of chemical reactions [8–11] or modify work functions [12], phase transitions [13], and (super-) conductivity [14–16], even without externally driving the cavity mode. However, theoretical support for such phenomena relies mainly on the analysis of phenomenological single-mode models (see, for example, Refs. [2–7] and references therein), which ignore the coupling to an infinite number of other vacuum modes. In turn, multimode models require the introduction of an *ad hoc* cutoff to avoid divergencies, which ends up affecting the results [17]. Thus, such models *per se* are incapable of making reliable predictions about the magnitude or even the sign of vacuum-induced energy shifts, and it remains unclear whether the nonperturbative regime is accessible at the level of individual dipoles.

In this Letter we investigate the ground-state energy shift of a single dipole due to its coupling to the electromagnetic vacuum in a confined geometry. Specifically, we focus on the two basic settings of a lumped-element LC resonator and a nanoplasmonic cavity, which are representative for a large variety of ultrastrong coupling experiments [3,4] and allow us to resolve this open problem by performing a cutoff-independent derivation of the vacuum-induced shifts of the ground state. These shifts can further be interpreted in terms of purely electrostatic effects and genuine vacuum corrections and studied as a function of the relevant system parameters in generic cavity QED setups. This analysis explicitly shows that, when relying on confinement only, the resulting energy shifts are dominated by electrostatic corrections, while contributions from dynamical modes remain perturbative at most. However, the effect of vacuum fluctuations can be strongly enhanced for electromagnetic modes with a high impedance, where the ratio between the electric and the magnetic field strength is modified compared with free space. This condition can be reached, for example, with appropriately designed lumped-element resonators or with plasmonic resonances, where the matter component contributes with a large kinetic inductance. Indeed, we find that, in both of the considered settings, nonperturbative shifts of the ground state, which are comparable to the bare transition frequency of the dipole, are feasible in principle. These predictions thus serve as an

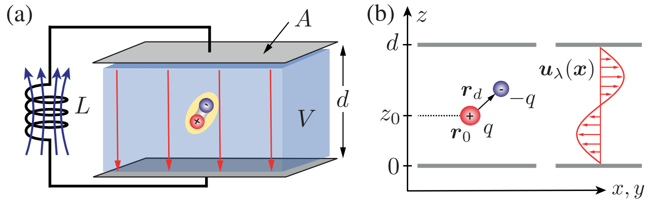

FIG. 1. (a) Sketch of a generic cavity QED system with a single dipole located in a strongly confined volume V between two metallic plates. The inductance L is used to model an additional external cavity mode with frequency $\omega_c = 1/\sqrt{LC}$ and impedance $Z = \sqrt{L/C}$, where $C = \epsilon_0 A/d$. (b) Coordinates of the two charges representing the dipole and sketch of a mode function of the transverse vector potential. See text and the Supplemental Material [18] for more details.

important guideline for designing experiments that can reach this regime as well as a benchmark for more refined models and numerical simulations of ultrastrong coupling physics.

QED in a confined geometry.—We first consider the setup shown in Fig. 1, where a single dipole is coupled to the quantized electromagnetic field in a volume V defined by two perfect metallic plates with area A and spacing d. Without loss of generality, we model the dipole as an effective particle of charge $-q$ and mass m, which is displaced by $\boldsymbol{r}_d = (x_d, y_d, z_d)$ from the opposite charge at a fixed position $\boldsymbol{r}_0 = (0, 0, z_0)$. The quantized field is represented, first of all, by an infinite set of transverse modes with frequencies ω_λ and mode functions $\boldsymbol{u}_\lambda$, which are determined by a vanishing potential at the boundaries, $\phi(\boldsymbol{x})|_{\partial V} = 0$. Further, we allow charges to flow freely between the two plates, which gives rise to one additional independent degree of freedom to account for a finite potential difference across the plates. This purely longitudinal mode represents our cavity mode of interest and can be modeled as an LC resonance with inductance L, capacitance $C = \epsilon_0 A/d$, and frequency $\omega_c = 1/\sqrt{LC}$. Therefore, in this setting, which is most relevant for cavity QED systems in the GHz and THz regime, the properties of the cavity mode can be engineered independently of the geometry of confinement.

In the nonrelativistic regime and under the validity of the dipole approximation, the full Hamiltonian describing this setup can be written as [18]

$$H = \sum_\lambda \hbar\omega_\lambda a_\lambda^\dagger a_\lambda + \hbar\omega_c a_c^\dagger a_c + H_{\rm dip}^0 + V_{\rm im}(\boldsymbol{r}_0, \boldsymbol{r}_d) + \frac{q}{m}\boldsymbol{A}(\boldsymbol{r}_0)\cdot\boldsymbol{p} + \frac{q^2}{2m}\boldsymbol{A}^2(\boldsymbol{r}_0) + \hbar g(a_c + a_c^\dagger)\mu + \frac{\hbar g^2}{\omega_c}\mu^2. \quad (1)$$

Here, the first two terms represent the transverse electromagnetic modes and the LC cavity mode with bosonic annihilation operators a_λ and a_c, respectively. The third term, $H_{\rm dip}^0 = \sum_j E_j |j\rangle\langle j|$, is the Hamiltonian of the dipole in free space, which we write in terms of its eigenstates $|j\rangle$ and eigenenergies E_j.

The confinement modifies the electromagnetic surrounding seen by the dipole, which, first of all, leads to a modification of the Coulomb potential by the metallic plates. In Eq. (1), this effect is included through $V_{\rm im}(\boldsymbol{r}_0, \boldsymbol{r}_d)$, which accounts for the additional interactions between the dipole and its image charges. Secondly, the boundaries modify the frequencies and mode functions of the transverse electromagnetic modes inside the volume $V = dA$ enclosed by the plates. In the Coulomb gauge, these modes couple to the momentum $\boldsymbol{p} = -i\hbar\boldsymbol{\nabla}_{\boldsymbol{r}_d}$ via the usual minimal coupling substitution. This gives rise to the $\boldsymbol{p}\cdot\boldsymbol{A}$ and $\boldsymbol{A}^2$ contributions in the second line of Eq. (1), where

$$\boldsymbol{A}(\boldsymbol{x}) = \sum_\lambda \sqrt{\frac{\hbar}{2\epsilon_0\omega_\lambda}}[\boldsymbol{u}_\lambda(\boldsymbol{x})a_\lambda + \boldsymbol{u}_\lambda^*(\boldsymbol{x})a_\lambda^\dagger] \quad (2)$$

is the vector potential. Note that, for a given geometry, the transverse mode functions $\boldsymbol{u}_\lambda$ and the electrostatic modifications $V_{\rm im}$ are related by the electromagnetic Green's function and cannot be treated independently of each other. Explicit expressions for $\boldsymbol{u}_\lambda$ and $V_{\rm im}$ for the considered setup are given in the Supplemental Material [18].

Finally, the dipole couples to the homogeneous electric field associated with the LC resonance, which is represented by the last two terms in Eq. (1). Here, we have defined the dimensionless dipole transition operator $\mu = z_d/a_0$, where $a_0 = |\langle 0|z_d|1\rangle|$ is the characteristic size of the dipole. The relevant coupling parameter can then be written as [20]

$$\eta = \frac{g}{\omega_c} = \frac{qa_0}{ed}\sqrt{2\pi\alpha\frac{Z}{Z_{\rm vac}}}, \quad (3)$$

where $\alpha \simeq 1/137$ is the fine-structure constant, $Z = \sqrt{L/C}$ is the resonator impedance, and $Z_{\rm vac} = 1/(\epsilon_0 c)$ is the impedance of free space. This way of expressing the coupling is convenient as it immediately shows that, although being intrinsically weak, light-matter interactions can be substantially enhanced by engineering modes with a high impedance, $Z \gg Z_{\rm vac}$. Such modes necessarily correspond to longitudinal modes and involve, for example, moving charges with a large kinetic inductance.

Ground-state energy shift.—A central quantity of interest in ultrastrong coupling cavity QED is the change in the ground-state energy, $E_{\rm GS}$, when the dipole is placed inside the cavity. For $\eta \lesssim 1$ this shift can be calculated by starting from the unperturbed ground state, $|j=0\rangle|{\rm vac}\rangle$, and treating all corrections in second-order perturbation theory. However, due to an infinite number of modes a_λ, the result of such a calculation will diverge or contain an explicit cutoff dependence when the number of modes is restricted [17,21]. This problem is known, for example, from the evaluation of Casimir-Polder forces [22] and can be resolved by keeping in mind that a similar divergence also occurs in free space while the observable energy difference $\Delta E_{\rm GS} = E_{\rm GS}|_{\rm cavity} - E_{\rm GS}|_{\rm free}$ remains finite. In the Supplemental Material [18] we present the details of this calculation, which results in a total energy shift of the form

$$\Delta E_{\rm GS} = \Delta E_{\rm im} + \Delta E_{\boldsymbol{A}} + \Delta E_{\rm cav}. \tag{4}$$

The individual contributions account for the purely electrostatic corrections and the genuine vacuum shifts from the transverse modes and the cavity mode, respectively. To make explicit predictions, we will evaluate these contributions for an isotropic harmonic dipole with frequency ω_0. Nevertheless, since the ground-state energy shift is dominated by the transition to the first-excited state, all results apply very accurately for more general systems with the same transition frequency and transition dipole moment.

In the limit $\sqrt{A} \gg d$, the image charge potential $V_{\rm im}$ can be evaluated analytically, and the resulting shift can be approximately written as [18]

$$\Delta E_{\rm im} \simeq -V_C \frac{a_0^3}{d^3} \mathcal{F}_{\rm im}(z_0/d), \tag{5}$$

where $V_C = q^2/(4\pi\epsilon_0 a_0)$ is the relevant Coulomb energy. The dimensionless function

$$\mathcal{F}_{\rm im}(x) = \frac{1}{8}\left[\frac{2}{x^3} - \Psi^{(2)}(1-x) - \Psi^{(2)}(1+x)\right], \tag{6}$$

where $\Psi^{(2)}(x)$ is the polygamma function, is plotted in Fig. 2(a). It assumes a minimal value of $\mathcal{F}_{\rm im}(1/2) \approx 4.21$ at the center of the cavity and scales as $\mathcal{F}_{\rm im}(z_0/d \to 0) \simeq d^3/(4z_0^3)$ for small z_0, where it reproduces the usual van der Waals energy of an atom in front of a single metallic plate.

The evaluation of the shift $\Delta E_{\boldsymbol{A}}$ from the transverse modes is more subtle [23] and only gives meaningful predictions once the corresponding free-space contribution is subtracted. Techniques to do so have originally been developed for calculating the Lamb shift [1] and Casimir-Polder forces [22,24,25], but have later been applied to cavity geometries as well [24,26–30]. Our analytic calculations of $\Delta E_{\boldsymbol{A}}$ in the Supplemental Material [18] follow closely the derivations presented in Ref. [27], but extended to the relevant limit of strong confinement, $\omega_0/\omega_\perp < 1$, where $\omega_\perp = \pi c/d$ is the frequency of the fundamental transverse mode and c is the speed of light. In addition, we use numerical summation to verify that all results are independent of the precise details of the cutoff function and already converge for rather low values of the cutoff scale $\Lambda \approx 5\omega_\perp$. This is a crucial observation, since it shows that none of the following results depends on the often unknown high-frequency properties of the model. From this analysis we obtain [18]

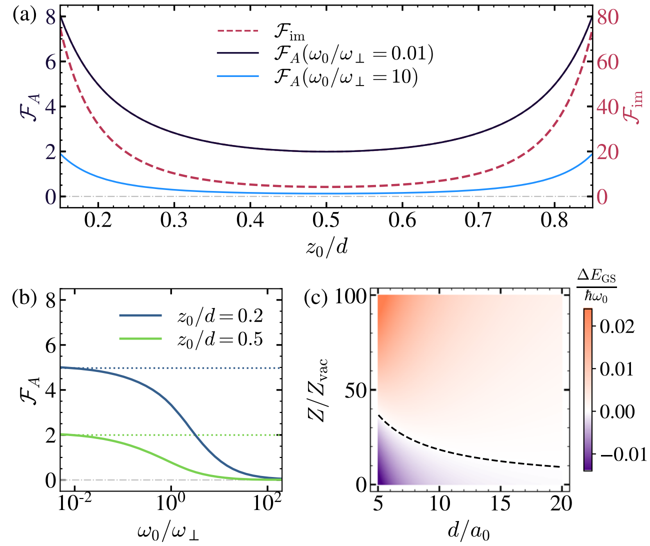

FIG. 2. (a) Dependence of the dimensionless functions $\mathcal{F}_{\rm im}$ and $\mathcal{F}_{\boldsymbol{A}}$ on the dipole position within the cavity, z_0/d. (b) Dependence of $\mathcal{F}_{\boldsymbol{A}}$ on the ratio $\omega_0/\omega_\perp$, where $\omega_\perp = \pi c/d$, for two different positions z_0/d. (c) Total value of the ground-state energy shift $\Delta E_{\rm GS}$ when the dipole is coupled to an LC resonance with impedance Z and the plates are separated by a distance d. For this plot a value of $z_0/d = 0.5$, $\hbar\omega_0 = V_C/2$, and $q = e$ have been assumed.

$$\Delta E_{\boldsymbol{A}} = \alpha\hbar\omega_0 \left(\frac{q a_0}{e d}\right)^2 \mathcal{F}_{\boldsymbol{A}}\left(\frac{\omega_0}{\omega_\perp}, \frac{z_0}{d}\right), \tag{7}$$

where the dimensionless scaling function $\mathcal{F}_{\boldsymbol{A}} > 0$ is plotted in Fig. 2(a). For $\omega_0 \to 0$ it assumes a value of $\mathcal{F}_{\boldsymbol{A}}(0, 1/2) = 2\pi/3$ at the center of the cavity and scales as $\mathcal{F}_{\boldsymbol{A}}(0, z_d/d \to 0) \simeq d^2/(2\pi z_0^2)$ near the plate. For $\omega_0 > \omega_\perp$, i.e., when retardation effects become important, this function decreases rapidly, as shown in Fig. 2(b).

From Eq. (7) we see that, compared to electrostatic effects, the overall energy shift resulting from all transverse modes is positive. This is an important finding and shows that for strong confinement, the positive energy correction from the $\boldsymbol{A}^2$ term dominates over the negative second-order shifts obtained from the $\boldsymbol{p} \cdot \boldsymbol{A}$ coupling. However, compared with electrostatics, the magnitude of $\Delta E_{\boldsymbol{A}}$ is suppressed by the fine-structure constant, and we obtain the bound

$$\begin{aligned}\frac{\Delta E_{\boldsymbol{A}}}{|\Delta E_{\rm im}|} &= \alpha \frac{\hbar\omega_0}{V_C}\frac{d}{a_0}\frac{\mathcal{F}_{\boldsymbol{A}}(\omega_0/\omega_\perp, z_0/d)}{\mathcal{F}_{\rm im}(z_0/d)} \\ &= \pi\frac{\omega_0}{\omega_\perp}\frac{\mathcal{F}_{\boldsymbol{A}}(\omega_0/\omega_\perp, z_0/d)}{\mathcal{F}_{\rm im}(z_0/d)} < 1,\end{aligned} \tag{8}$$

which holds in all parameter regimes [18]. This observation is consistent with the fact that Casimir-Polder forces between a dipole and a metallic plate are attractive and shows that even an extreme confinement, $d \sim a_0$, does not change this result. Equation (7) also implies that for any $d > a_0$ the combined vacuum shift resulting from all transverse modes is only a small fraction of the bare transition frequency, ω_0.

The third term in Eq. (4) arises from the coupling of the dipole to the additional LC resonance. This mode is absent in free space, and therefore we can use standard perturbation theory to obtain

$$\Delta E_{\rm cav} = -\frac{\hbar g^2}{\omega_c + \omega_0} + \frac{\hbar g^2}{\omega_c}. \tag{9}$$

In the limit $\omega_0 \ll \omega_c$ and using Eq. (3), we can write this contribution as

$$\Delta E_{\rm cav} \simeq \alpha\hbar\omega_0 \left(\frac{q a_0}{ed}\right)^2 \frac{Z}{Z_{\rm vac}} \mathcal{F}_{\rm cav}, \tag{10}$$

with a numerical factor $\mathcal{F}_{\rm cav} = 2\pi$. Like for the transverse modes, the vacuum shift induced by the LC resonance is positive and has the same scaling with frequency and distance d. The overall magnitude, however, is enhanced by the ratio $Z/Z_{\rm vac}$, which can be used to compensate for the small value of the fine-structure constant.

For GHz resonators, values of $Z/Z_{\rm vac} \sim 50$–80 have already been demonstrated using optimized geometric inductors [31] or superinductors [32]. Although experimentally challenging, Eq. (10) implies that under such conditions, nonperturbative vacuum shifts, $\Delta E_{\rm cav}/(\hbar\omega_0) \sim 1$, are in principle accessible. As illustrated in Fig. 2(c), the coupling to such high-impedance modes can also result in "anomalous" vacuum shifts, $\Delta E_{\rm GS} > 0$, where the positive contribution from the dynamical modes exceeds electrostatic effects. This is very intriguing, as such a positive shift implies an outward vacuum pressure on the cavity mirrors, in contrast to the attractive Casimir force arising from the zero-point energy of the electromagnetic modes [33]. However, in contrast to related previous predictions [21], we find that the experimental conditions for accessing this regime are rather extreme, and more refined studies will be necessary to assess the role of such effects for potential applications.

Plasmonic nanosphere cavity.—In the previous setup we have assumed perfect metallic boundary conditions and thereby ignored dynamical electromagnetic modes associated with the redistribution of electrons inside the metal. In our second example we specifically address the influence of these excitations and consider the setup shown in Fig. 3(a), where the dipole is placed at a distance z_0 above the surface of a plasmonic nanosphere cavity with radius R. Following Ref. [34], we model the electrons inside this sphere as an

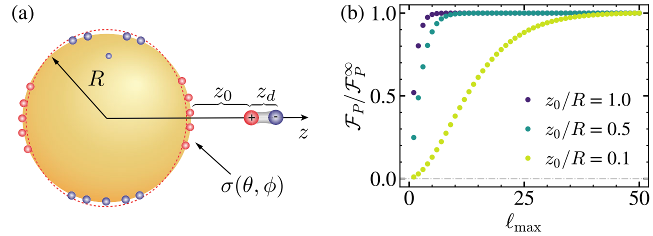

FIG. 3. (a) Sketch of a dipole located a distance z_0 above the surface of a plasmonic nanosphere cavity with radius R and surface charge density σ. (b) Plot of the function $\mathcal{F}_P$ defined in Eq. (15) versus the cutoff $\ell_{\max}$, where $\mathcal{F}_P^\infty$ denotes the asymptotic value for $\ell_{\max} \to \infty$. For these plots $\omega_0/\omega_P = 1$ and different values of z_0 have been assumed.

incompressible fluid of density n_0, which exhibits a discrete set of plasmon modes with frequencies $\omega_\ell = \omega_P\sqrt{\ell/(2\ell+1)}$. Here, $\omega_P = \sqrt{e^2 n_0/(m_e\epsilon_0)}$ is the plasma frequency and m_e is the electron mass. These modes describe excitations of the surface charge density σ with an angular momentum quantum number ℓ. By restricting the motion of the dipole along the z axis for simplicity, the Hamiltonian for this setup is [18]

$$H = H_{\rm dip}^0 + V_{\rm im} + \hbar\sum_{\ell=1}^{\ell_{\max}} \left[\omega_\ell a_\ell^\dagger a_\ell + g_\ell(a_\ell + a_\ell^\dagger)\mu + \frac{g_\ell^2}{\omega_\ell}\mu^2\right], \tag{11}$$

where $V_{\rm im} \equiv V_{\rm im}(z_0, z_d)$ denotes the image potential experienced by a static dipole in front of the sphere. In Eq. (11), a_ℓ ($a_\ell^\dagger$) are the annihilation (creation) operators for the plasmon modes up to a maximal quantum number $\ell_{\max}$, and we have defined the coupling constants $g_\ell = g_P\sqrt[4]{\ell(\ell+1)^4/(2\ell+1)}[R/(R+z_0)]^{\ell+2}/2$. Here,

$$\eta_P = \frac{g_P}{\omega_P} = \frac{q a_0}{eR}\sqrt{2\pi\alpha\frac{Z_P}{Z_{\rm vac}}} \tag{12}$$

and $Z_P = (\pi\epsilon_0 R\omega_P)^{-1}$ is the characteristic impedance. Note that Eq. (11) has been derived starting from Coulomb interactions only, and therefore neglects small corrections from the coupling to transverse modes, which we have already evaluated above. In the limit $\ell_{\max} \to \infty$, the so-called P^2 term, $\sum_\ell g_\ell^2\mu^2/\omega_\ell$, cancels the instantaneous image potential, $V_{\rm im}$, exactly. However, by writing Eq. (11) in this canonical form one avoids a double-counting of electrostatic interactions also for a finite number of modes, and one recovers the correct single-mode cavity QED Hamiltonian for $\ell_{\max} = 1$ [20].

Since the plasmon modes are absent in free space, the ground-state shift resulting from Hamiltonian (11) is given by $\Delta E_{\rm GS} \simeq \Delta E_{\rm im} + \Delta E_P$. Here, $\Delta E_{\rm im}$ accounts again for the electrostatic contribution $\sim V_{\mathrm{im}}$, which in the limit $z_0/R \ll 1$ reduces to the van der Waals interaction [18]

$$\Delta E_{\mathrm{im}}(z_0 \ll R) \simeq -\frac{q^2 a_0^2}{4\pi\epsilon_0 (2z_0)^3} \tag{13}$$

for a dipole oriented along the z direction. The energy shift resulting from the coupling to the dynamical plasmon modes can be written as

$$\Delta E_P \simeq \alpha\hbar\omega_0 \left(\frac{qa_0}{ez_0}\right)^2 \frac{Z_{\mathrm{eff}}(z_0)}{Z_{\mathrm{vac}}} \mathcal{F}_P\left(\frac{\omega_0}{\omega_P}, \frac{z_0}{R}\right), \tag{14}$$

where $Z_{\mathrm{eff}}(z_0) = (\pi\epsilon_0 z_0 \omega_P)^{-1}$ and

$$\mathcal{F}_P(x,y) = \frac{\pi y^3}{2} \sum_{\ell=1}^{\ell_{\max}} \frac{(\ell+1)^2\sqrt{(2\ell+1)/\ell}}{1 + x\sqrt{(2\ell+1)/\ell}} \left(\frac{1}{1+y}\right)^{2\ell+4}. \tag{15}$$

In Fig. 3(b) we plot the value of this function for increasing $\ell_{\max}$ and show that it converges to a finite value $\mathcal{F}_P^\infty(x,y)$ for a sufficiently large $\ell_{\max}$. This demonstrates that also in this scenario we can obtain an unambiguous result for the ground-state energy shift that does not depend on an *ad hoc* mode truncation. However, Fig. 3(b) also shows that, for $z_0 < R$, a single-mode cavity QED model would be insufficient to predict this shift accurately.

In Eq. (14), we have combined the contribution from all plasmon modes into an effective impedance $Z_{\mathrm{eff}}(z_0)$, which shows that for small dipole-sphere separations, z_0 replaces the radius R as the relevant length scale. In this limit, $\mathcal{F}_P^\infty(x \ll 1, y \ll 1) \simeq \pi/\sqrt{32}$. For plasma frequencies in the range of 1–10 eV [35,36] and $z_0 = 0.5$ nm [37,38] we obtain $Z_{\mathrm{eff}}/Z_{\mathrm{vac}} \approx 12$–125, which for a large molecule with $qa_0/(ez_0) \approx 1$ corresponds to $\Delta E_P/(\hbar\omega_0) \approx 0.05$–0.50, still assuming that $\omega_0 \lesssim \omega_P$. Therefore, also in the plasmonic case, nonperturbative vacuum effects are within experimental reach. Note, however, that since $Z_{\mathrm{eff}}(z_0)$ is fixed by geometry and cannot be engineered independently, we find that the total shift in this setup, $\Delta E_{\mathrm{im}} + \Delta E_P < 0$, is negative for all values of z_0 and ω_0 [18].

Summary and conclusions.—In summary, we have presented an *ab initio* and cutoff-independent derivation of the total ground-state energy shift in two prototypical cavity QED settings. By focusing on simple geometries, we have obtained analytic predictions for the dependence of this shift on the most relevant experimental parameters and provided a clear distinction between purely electrostatic corrections and genuine vacuum effects. Our results demonstrate that the coupling to strongly confined transverse modes, as often considered in cavity QED, is not enough to induce significant perturbations of the ground state. The main effect of the confinement is electrostatic modifications, which in turn are often neglected in this context. These findings are consistent with the previous literature on Casimir-Polder interactions and establish a direct link between those closely related, but so far largely disconnected fields of research.

However, going beyond such conventional settings, our analysis predicts a significant enhancement of vacuum corrections in the presence of high-impedance modes. Under such conditions, the regime of nonperturbative cavity QED [20], with its many intriguing phenomena [39–49], comes within experimental reach. The very general current analysis can help to guide further experimental and theoretical progress in this direction.

This work was supported by the Austrian Science Fund (FWF) through Grant No. P31701 (ULMAC), Grant No. P32299 (PHONED), and the ESPRIT fellowship ESP 230-N (mesoQED). D. B. acknowledges support by the Provincia Autonoma di Trento. J. F. acknowledges support by the European Research Council through Grant ERC-2016-STG-714870 and by the Spanish Ministry for Science, Innovation, and Universities–Agencia Estatal de Investigación through Grants No. PID2021-125894NB-I00 and No. CEX2018-000805-M (through the María de Maeztu program for Units of Excellence in Research and Development).

[1] H. Bethe, The electromagnetic shift of energy levels, Phys. Rev. **72**, 339 (1947).

[2] R. F. Ribeiro, L. A. Martinez-Martinez, M. Du, J. Campos-Gonzalez-Angulo, and J. Yuen-Zhou, Polariton chemistry: controlling molecular dynamics with optical cavities, Chem. Sci. **9**, 6325 (2018).

[3] P. Forn-Díaz, L. Lamata, E. Rico, J. Kono, and E. Solano, Ultrastrong coupling regimes of light-matter interaction, Rev. Mod. Phys. **91**, 025005 (2019).

[4] A. F. Kockum, A. Miranowicz, S. De Liberato, S. Savasta, and F. Nori, Ultrastrong coupling between light and matter, Nat. Rev. Phys. **1**, 19 (2019).

[5] F. J. Garcia-Vidal, C. Ciuti, and T. W. Ebbesen, Manipulating matter by strong coupling to vacuum fields, Science **373**, eabd0336 (2021).

[6] F. Schlawin, D. M. Kennes, and M. A. Sentef, Cavity quantum materials, Appl. Phys. Rev. **9**, 011312 (2021).

[7] M. Ruggenthaler, D. Sidler, and A. Rubio, Understanding polaritonic chemistry from *ab initio* quantum electrodynamics, arXiv:2211.04241.

[8] J. A. Hutchison, T. Schwartz, C. Genet, E. Devaux, and T. W. Ebbesen, Modifying chemical landscapes by coupling to vacuum fields, Angew. Chem., Int. Ed. Engl. **51**, 1592 (2012).

[9] A. Thomas, J. George, A. Shalabney, M. Dryzhakov, S. J. Varma, J. Moran, T. Chervy, X. Zhong, E. Devaux, C. Genet, J. A. Hutchison, and T. W. Ebbesen, Ground-state chemical reactivity under vibrational coupling to the vacuum electromagnetic field, Angew. Chem., Int. Ed. Engl. **55**, 11462 (2016).

[10] A. Thomas, L. Lethuillier-Karl, K. Nagarajan, R. M. A. Vergauwe, J. George, T. Chervy, A. Shalabney, E. Devaux, C. Genet, J. Moran, and T. W. Ebbesen, Tilting a ground-state reactivity landscape by vibrational strong coupling, Science **363**, 615 (2019).

[11] K. Hirai, R. Takeda, J. A. Hutchison, and H. Uji-i, Modulation of Prins cyclization by vibrational strong coupling, Angew. Chem., Int. Ed. Engl. **59**, 5332 (2020).

[12] J. A. Hutchison, A. Liscio, T. Schwartz, A. Canaguier-Durand, C. Genet, V. Palermo, S. Samorì, and T. W. Ebbesen, Tuning the work-function via strong coupling, Adv. Mater. **25**, 2481 (2013).

[13] S. Wang, A. Mika, J. A. Hutchison, C. Genet, A. Jouaiti, M. W. Hosseini, and T. W. Ebbesen, Phase transition of a perovskite strongly coupled to the vacuum field, Nanoscale **6**, 7243 (2014).

[14] A. Thomas, E. Devaux, K. Nagarajan, T. Chervy, M. Seidel, D. Hagenmüller, S. Schütz, J. Schachenmayer, C. Genet, G. Pupillo, and T. W. Ebbesen, Exploring superconductivity under strong coupling with the vacuum electromagnetic field, arXiv:1911.01459.

[15] G. L. Paravicini-Bagliani, F. Appugliese, E. Richter, F. Valmorra, J. Keller, M. Beck, N. Bartolo, C. Rössler, T. Ihn, K. Ensslin, C. Ciuti, G. Scalari, and J. Faist, Magneto-transport controlled by Landau polariton states, Nat. Phys. **15**, 186 (2019).

[16] F. Appugliese, J. Enkner, G. L. Paravicini-Bagliani, M. Beck, C. Reichl, W. Wegscheider, G. Scalari, C. Ciuti, and J. Faist, Breakdown of topological protection by cavity vacuum fields in the integer quantum Hall effect, Science **375**, 1030 (2022).

[17] N. M. Hoffmann, L. Lacombe, A. Rubio, and N. T. Maitra, Effect of many modes on self-polarization and photochemical suppression in cavities, J. Chem. Phys. **153**, 104103 (2020).

[18] See Supplemental Material at http://link.aps.org/supplemental/10.1103/PhysRevLett.131.013602, which includes the additional Ref. [19], for more details about the model and the derivation of all the analytic results.

[19] K. Takae and A. Onuki, Applying electric field to charged and polar particles between metallic plates: Extension of the Ewald method, J. Chem. Phys. **139**, 124108 (2013).

[20] D. De Bernardis, T. Jaako, and P. Rabl, Cavity quantum electrodynamics in the non-perturbative regime, Phys. Rev. A **97**, 043820 (2018).

[21] V. Rokaj, M. Ruggenthaler, F. G. Eich, and A. Rubio, Free electron gas in cavity quantum electrodynamics, Phys. Rev. Res. **4**, 013012 (2022).

[22] H. B. G. Casimir and D. Polder, The influence of retardation on the London-van der Waals forces, Phys. Rev. **73**, 360 (1948).

[23] P. W. Milonni, *The Quantum Vacuum* (Academic Press, New York, 1994).

[24] I. E. Dzyaloshinskii, E. M. Lifshitz, and L. P. Pitaevskii, The general theory of van der Waals forces, Adv. Phys. **10**, 165 (1961).

[25] J. M. Wylie and J. E. Sipe, Quantum electrodynamics near an interface, Phys. Rev. A **30**, 1185 (1984).

[26] H. B. G. Casimir, On the attraction between two perfectly conducting plates, Kon. Ned. Akad. Wetensch. Proc. **51**, 793 (1948).

[27] G. Barton, Quantum electrodynamics of spinless particles between conducting plates, Proc. R. Soc. A **320**, 251 (1970).

[28] E. A. Power and T. Thirunamachandran, Quantum electrodynamics in a cavity, Phys. Rev. A **25**, 2473 (1982).

[29] K. Svozil, Mass and Anomalous Magnetic Moment of an Electron between Two Conducting Parallel Plates, Phys. Rev. Lett. **54**, 742 (1985).

[30] D. Reiche, K. Busch, and F. Intravaia, Nonadditive Enhancement of Nonequilibrium Atom-Surface Interactions, Phys. Rev. Lett. **124**, 193603 (2020).

[31] M. Peruzzo, A. Trioni, F. Hassani, M. Zemlicka, and J. M. Fink, Surpassing the Resistance Quantum with a Geometric Superinductor, Phys. Rev. Appl. **14**, 044055 (2020).

[32] R. Kuzmin, R. Mencia, N. Grabon, N. Mehta, Y.-H. Lin, and V. E. Manucharyan, Quantum electrodynamics of a superconductor–insulator phase transition, Nat. Phys. **15**, 930 (2019).

[33] By assuming fixed boundaries, the Casimir force [26] is not included in our discussion, but can be readily taken into account by adding the electromagnetic zero-point energy, $\sum_\lambda \hbar\omega_\lambda/2 + \hbar\omega_c/2$, to the Hamiltonian in Eq. (1).

[34] E. Prodan and P. Nordlander, Plasmon hybridization in spherical nanoparticles, J. Chem. Phys. **120**, 5444 (2004).

[35] C. Kittel, *Introduction to Solid State Physics*, 8th ed. (John Wiley & Sons, Inc., New York, 2004).

[36] G. V. Naik, V. M. Shalaev, and A. Boltasseva, Alternative plasmonic materials: Beyond gold and silver, Adv. Mater. **25**, 3264 (2013).

[37] R. Chikkaraddy, B. de Nijs, F. Benz, S. J. Barrow, O. A. Scherman, E. Rosta, A. Demetriadou, P. Fox, O. Hess, and J. J. Baumberg, Single-molecule strong coupling at room temperature in plasmonic nanocavities, Nature (London) **535**, 127 (2016).

[38] M. Kuisma, B. Rousseaux, K. M. Czajkowski, T. P. Rossi, T. Shegai, P. Erhart, and T. J. Antosiewicz, Ultrastrong coupling of a single molecule to a plasmonic nanocavity: A first-principles study, ACS Photonics **9**, 1065 (2022).

[39] A. Ridolfo, S. Savasta, and M. J. Hartmann, Nonclassical Radiation from Thermal Cavities in the Ultrastrong Coupling Regime, Phys. Rev. Lett. **110**, 163601 (2013).

[40] J. Galego, F. J. Garcia-Vidal, and J. Feist, Cavity-Induced Modifications of Molecular Structure in the Strong-Coupling Regime, Phys. Rev. X **5**, 041022 (2015).

[41] J. Flick, M. Ruggenthaler, H. Appel, and A. Rubio, Atoms and molecules in cavities, from weak to strong coupling in quantum-electrodynamics (QED) chemistry, Proc. Natl. Acad. Sci. U.S.A. **114**, 3026 (2017).

[42] L. A. Martinez-Martinez, R. F. Ribeiro, J. Campos-Gonzalez-Angulo, and J. Yuen-Zhou, Can ultrastrong coupling change ground-state chemical reactions?, ACS Photonics **5**, 167 (2018).

[43] F. Schlawin, A. Cavalleri, and D. Jaksch, Cavity-Mediated Electron-Photon Superconductivity, Phys. Rev. Lett. **122**, 133602 (2019).

[44] N. Rivera, J. Flick, and P. Narang, Variational Theory of Nonrelativistic Quantum Electrodynamics, Phys. Rev. Lett. **122**, 193603 (2019).

[45] M. Schuler, D. De Bernardis, A. M. Läuchli, and P. Rabl, The vacua of dipolar cavity quantum electrodynamics, SciPost Phys. **9**, 066 (2020).

[46] P. Pilar, D. De Bernardis, and P. Rabl, Thermodynamics of ultrastrongly coupled light-matter systems, Quantum **4**, 335 (2020).

[47] J. Li and M. Eckstein, Manipulating Intertwined Orders in Solids with Quantum Light, Phys. Rev. Lett. **125**, 217402 (2020).

[48] Y. Ashida, A. Imamoglu, and E. Demler, Cavity Quantum Electrodynamics at Arbitrary Light-Matter Coupling Strengths, Phys. Rev. Lett. **126**, 153603 (2021).

[49] R. C. Couto and M. Kowalewski, Suppressing non-radiative decay of photochromic organic molecular systems in the strong coupling regime, Phys. Chem. Chem. Phys. **24**, 19199 (2022).